https://doi.org/10.5194/egusphere-2026-3112
Preprint. Discussion started: 10 July 2026


# On the Role of Atmospheric Waves in Governing the Persistence of Thin Cirrus Clouds in the Tropical Tropopause Layer

Milena Corcos[1], Bernd Kärcher[2], Thomas Lesigne[3], Aurélien Podglajen[4], and Eric Jensen[5]

[1]NorthWest Research Associates, Boulder, CO, USA.
[2]Institut für Physik der Atmosphäre, DLR Oberpfaffenhofen, Wessling, Germany
[3]LATMOS/IPSL, Sorbonne Université, UVSQ, CNRS, Paris, France
[3]LATMOS/IPSL, Sorbonne Université, UVSQ, CNRS, Paris, France
[4]LMD/IPSL, École Polytechnique - Institut Polytechnique de Paris, Sorbonne Université, École Normale Supérieure, CNRS
[5]NOAA Chemical Sciences Laboratory, Boulder, CO, USA

**Correspondence:** Milena Corcos (milena@nwra.com)

**Abstract.** Thin tropical cirrus clouds influence the radiative and stratospheric water vapor budgets, yet the processes controlling their persistence remain poorly constrained. Here, we investigate the impact of multiscale wave-driven vertical wind speed and temperature fluctuations on thin tropical cirrus lifetime using a Lagrangian microphysical model initialized from lidar observations obtained during the Strateole-2 campaigns. The model represents the evolution of ice crystal populations under stochastic high-frequency gravity wave forcing and an idealized low-frequency inertia gravity wave. Our results show that cirrus lifetime is controlled by a competition between stabilization through multiscale cooling fluctuations and complete sublimation by rare, high amplitude warming events due to gravity waves. This introduces a threshold behavior: if some ice crystals can grow large enough without being dissipated in the first hours of the lifetime, they become less sensitive to complete sublimation and enter a stabilization regime in which sedimentation determines the cloud lifetime. Stronger gravity-wave activity shifts this stabilization regime toward larger crystal sizes and generally shortens cirrus lifetime. Lower frequency waves modulate this evolution by setting the slowly varying background temperature. Cooling phases promote crystal growth and favor long-lived cirrus, while warming phases enhance rapid cloud decay. The simulated lifetime distribution reproduces the strongly skewed distribution of observed thin tropical cirrus lifetimes, including a non negligible population of clouds which persists longer than 12 h, and dominates the total cloud coverage.

## 1 Introduction

Thin cirrus clouds near the tropical tropopause layer (TTL) play an essential role in Earth's climate system. We refer here to thin cirrus as optically and geometrically thin ice clouds formed in situ in the upper troposphere, where weak ascent and low temperatures maintain high relative humidity over large regions (Jensen et al., 1999; McFarquhar et al., 2000; Pfister et al., 2001; Dessler et al., 2006). These ice clouds impact the stratospheric water budget as well as the radiative budget due to their frequent and widespread occurrence. They absorb terrestrial long-wave radiation and emit it at very low temperatures, producing localized heating and contributing to a net positive radiative forcing of approximately 0.7 $\mathrm{W\,m^{-2}}$ (McFarquhar et al.,

https://doi.org/10.5194/egusphere-2026-3112
Preprint. Discussion started: 10 July 2026


2000), ∼ 6% of tropical cirrus total radiative effect (Gasparini et al., 2025). However, the magnitude of this forcing remains uncertain due to the limited observations of these clouds. Since both dehydration efficiency and radiative impact are integrated over the cloud lifetime, constraining TTL cirrus persistence is critical to understanding their overall climate impact.

Recent long-duration lidar observations provide a new observational benchmark for studying thin cirrus clouds. Indeed, during the second Stratéole-2 campaign (2021–2022), three Balloonborne Cloud Observing micrOLidar (BeCOOL) aboard super-pressure balloons (SPB) provided the first continuous, high-resolution, semi-Lagrangian measurements of TTL cirrus across the tropical belt from the Indian Ocean to the central Pacific. These observations highlighted the ubiquity of very thin cirrus layers that are not well observed remotely (Lesigne et al., 2024). Using these new observations, Lesigne et al. (2025) inferred a highly skewed apparent lifetime distribution of thin cirrus clouds. They showed that although short-lived clouds dominate in number, the overall cirrus coverage, and thus the radiative impact, is primarily governed by the rarer, long-lived clouds that can persist for more than 12 h.

Numerous modeling studies have explored the dynamical, radiative, and microphysical processes that affect these clouds (Jensen et al., 1996, 2011, 2012; Dinh et al., 2010; Dinh and Fueglistaler, 2014; Podglajen et al., 2016, 2018; Corcos et al., 2023; Jensen et al., 2026). These simulations have revealed complex interactions between radiation, microphysics, and dynamics. At high frequencies, vertical velocity and temperature fluctuations associated with gravity waves (GW) strongly modulate homogeneous ice nucleation and the number concentration of ice crystals (Kärcher, 2003; Jensen and Pfister, 2004; Hoyle et al., 2005). SPB observations quantified the GW temperature perturbations to be on the order of 1 K (Podglajen et al., 2016; Schoeberl et al., 2017; Corcos et al., 2021). These perturbations can trigger ice nucleation events and shape cirrus characteristics (Dinh et al., 2016; Jensen et al., 2016; Spichtinger and Krämer, 2013; Jensen et al., 2026).

At lower frequencies, planetary and equatorial waves also modulate TTL cirrus occurrence and structure. Temperature anomalies associated with Kelvin, Rossby, mixed Rossby–gravity waves and inertia-gravity waves influence cirrus formation frequency and vertical extent (Boehm and Verlinde, 2000; Immler et al., 2008; Kim et al., 2016; Sweeney and Fu, 2023; Cao et al., 2025). TTL cirrus clouds are frequently observed within the cold phases of these waves, where weak ascent sustains supersaturation but may not trigger nucleation directly. Additionally, wind shear, wave-driven temperature variability, and radiative heating-induced mesoscale circulations further influence the structure and longevity of these clouds (Dinh et al., 2010; Jensen et al., 2025).

While both gravity waves and planetary waves are known to affect TTL cirrus, their combined impact on the cloud life cycle has not yet been studied at the process level. In this work, we investigate how multiscale wave forcing (combining low-frequency planetary waves and higher-frequency GW) controls the persistence of thin cirrus clouds in the TTL. Using recent observations of tropical waves and cirrus properties, we conduct process-based numerical simulations that resolve and couple these multiscale dynamical forcings. This study complements the observational findings of Lesigne et al. (2025) by disentangling the roles of different wave types in cirrus evolution, and extends previous modeling work (Jensen et al., 2016; Podglajen et al., 2018; Luo et al., 2003) by resolving the complete life cycle of TTL cirrus under realistic multiscale conditions. Our goal is to clarify how interactions between atmospheric waves and microphysical processes shape the evolution and persistence of thin tropical cirrus.

https://doi.org/10.5194/egusphere-2026-3112
Preprint. Discussion started: 10 July 2026


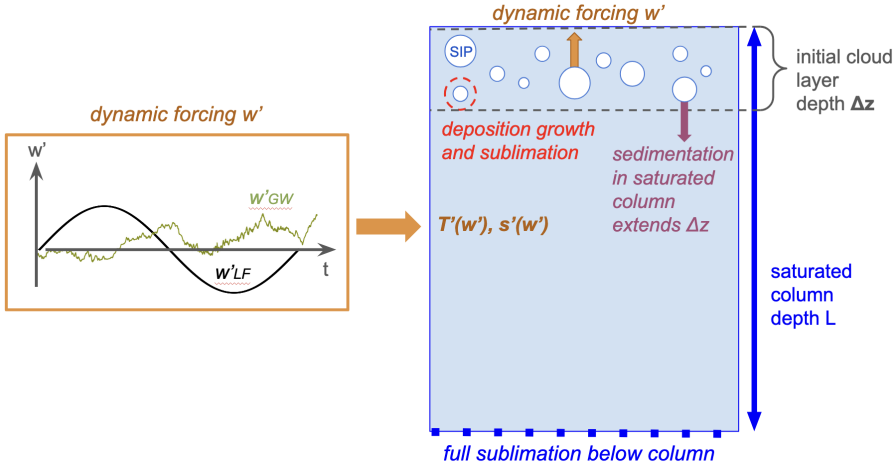


**Figure 1.** Schematic illustrating the key model features: the microphysical processes in the TTL cirrus layer of evolving depth $\Delta z$, the ice-saturated air column of constant depth $L$ in which the cloud layer evolves ($\Delta z \leq L$), and the gravity wave and low frequency wave forcings ($w'_{\mathrm{GW}}$ and $w'_{\mathrm{LF}}$, respectively) impacting the motion of the SIPs and the state variables of the column.

The paper is structured as follows: section 2 explains our model and initial conditions. Section 3 shows results from simulations that use only GW and in a second part combine it with the forcing of a lower frequency inertia-gravity wave. Section 4 elaborates on how our simulation results can be compared with the BeCOOL micro-lidar observations. Section 5 summarizes and discusses our main findings to conclude our study.

## 2 Microphysical-dynamical cirrus model

We study factors controlling the lifetimes of thin TTL cirrus clouds by means of a process-based cloud model (section 2.1), designed to simulate statistical distributions of associated lifetimes. The model is constrained by observations and dynamically forced by tropical waves (section 2.2). The initialization and our choice of key model parameters (section 2.3) are designed to replicate the atmospheric conditions encountered during the observation of such thin clouds near the tropical tropopause by the balloon-borne BeCOOL lidar measurements (Lesigne et al., 2024).

### 2.1 Description of the cirrus layer

Our model is derived from a cloud model we have developed recently to study contrail cirrus lifetime statistics. The equations governing the cloud ice microphysical processes and those connecting vertical air and particle motions with the resulting temperature and supersaturation changes are explained in detail in Kärcher and Corcos (2025).

As illustrated in Fig. 1, the model follows the evolution of a cirrus layer of depth $\Delta z$ that evolves within a saturated column of depth $L$ and tracks the Lagrangian altitude ($z$), number concentration ($n$), and radius ($r$) of cirrus ice crystals.

https://doi.org/10.5194/egusphere-2026-3112
Preprint. Discussion started: 10 July 2026


The simulations include dynamical forcings that generate time-dependent vertical wind fluctuations ($w'$) associated with high-frequency GW (periods of minutes to a day) and low frequency waves (LF) with a period of several days. The associated wave-driven dry-adiabatic temperature perturbations ($T'$) modulate ice supersaturation ($s'$), thereby driving deposition growth and sublimation. The vertical motion of ice crystals is thus determined by the superposition of sedimentation and vertical wind fluctuations ($w'$) .

The water vapor in the column is initially at ice saturation. Gravity-wave forcing induces transient fluctuations in supersaturation ($s' > 0$) and subsaturation ($s' < 0$) on timescales ranging from minutes to a few hours, while the long-term mean state remains close to ice saturation. Across the lifespan of TTL cirrus, this average value can only be changed by slow cooling or warming due to LF waves. $L$ represents the thickness of this ice-saturated column in the TTL where the cirrus layer can expand vertically, due to the sedimentation of ice crystals.

A large ensemble of simulation ice particles (SIP) represents the cirrus microphysical population. Each SIP stands for multiple real ice crystals sharing the same properties, with equal statistical weight, and experiencing the same thermodynamic and dynamical environment. The column and the cirrus layer evolving within it are one homogeneous environment, and the model does not account for a vertical structure. As sedimentation proceeds, the cirrus layer gradually deepens until SIPs settle below the column and are removed from the simulation, assuming that they would fully sublimate. Full sublimation of ice crystals is the only other ice loss mechanism in our model. The total water content is conserved during growth and sublimation but can irreversibly decrease due to sedimentation out of the domain.

The cirrus lifetime is defined as the time interval during which a threshold small number of SIPs remains within the column.

Horizontal advection is not explicitly represented in our model. SIP cannot move laterally out of the column, and the effects of vertical wind shear are therefore neglected. Lateral exchange between cloudy and surrounding air due to turbulent mixing is thus also not included. To estimate temperature changes from cloud radiative heating, we applied a simplified radiative transfer parameterization (Corti and Peter, 2009). For the optically very thin TTL cirrus analyzed here (optical depth $< 2 \cdot 10^{-3}$), radiative heating rates are found to be negligible compared to temperature perturbations from low-frequency waves (see Appendix A). Consequently, effects of radiative heating on the dynamics of the cirrus layers are omitted in the present simulations.

### 2.2 Multiscale wave forcing

Because GW are ubiquitous in the TTL (Corcos et al., 2021), all simulations include rapid vertical wind speed fluctuations associated with their activity. In previous studies, time series of $w'_{GW}(t)$ have been derived directly from continuous superpressure balloons (SPB) measurements. Those time series are polluted at frequencies approaching the local buoyancy frequency, due to contributions from non geophysical balloon natural oscillations (Podglajen et al., 2016). This issue was partly circumvented by filtering out variability above the buoyancy frequency (Dinh et al., 2016; Jensen et al., 2016, 2026), with the limitation of removing actual variability together with measurement artifacts. Furthermore, the available TTL dataset, covering about 241 days, is too short to provide robust statistics for our cirrus lifetime analysis.

https://doi.org/10.5194/egusphere-2026-3112
Preprint. Discussion started: 10 July 2026


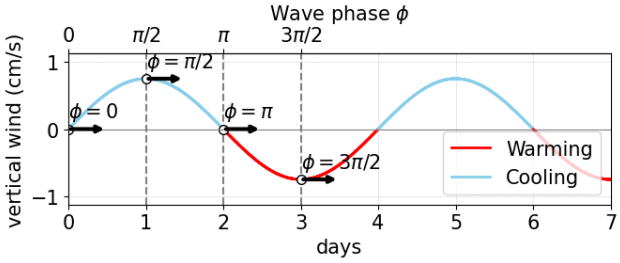


**Figure 2.** Schematic illustrating the low frequency (LF) forcing. The different arrows indicate the initial vertical wind speed for the different phase scenarios.

Instead, we use a parameterization that generates synthetic, stochastic time series of $w'_{GW}$, representative of continuous SPB observations of GW activity (Kärcher and Podglajen, 2019). In this approach, wave-induced vertical wind speed fluctuations are characterized by their standard deviation ($\sigma_w$) and autocorrelation time ($t_a$). The intrinsic periods of vertically propagating GW are bounded by the local buoyancy period, $\tau = 2\pi/N$, where $N$ is the Brunt–Väisälä frequency. For TTL conditions during the balloon flights, we adopt $N = 0.023$ s$^{-1}$, corresponding to $\tau \approx 4.5$ min. Based on the $N$-filtered superpressure balloons (SPB) data, we estimate an average $\sigma_w = 12$ cm s$^{-1}$ and $t_a \approx \tau/2$. may underestimate specific enhancements near the buoyancy frequency, e.g., due to trapped waves, which have been recently reported in the TTL from radar data (Kottayil et al., 2024). Furthermore, observed $\sigma_w$-values vary considerably along individual balloon flight segments (Jensen et al., 2026), and the data include intermittent high-amplitude wave packets that are not explicitly represented in the parameterization. To account for some of the variability, we explore the sensitivity of simulated cirrus lifetimes to $\sigma_w$ observed in different parts of the tropical band.

As cirrus clouds are often observed in large scale cold anomalies (e.g., Boehm and Verlinde, 2000; Immler et al., 2008), we also introduce a large scale, low frequency dynamical forcing. We represent the LF forcing by fitting the inertia gravity wave, observed by the SPB and described in Cao et al. (2025), to a monochromatic (sinusoidal) vertical wind speed perturbation ($w'_{\mathrm{LF}}$). This choice is motivated by observations showing a TTL cirrus embedded within the cold phase of this wave, for which the dynamical characteristics are well documented (Cao et al., 2025). The choice of the amplitude influences the range of temperatures experienced by the cirrus layer. The wave phase ($\phi$) impacts the evolution of ice crystals by shifting the onset of periods of cooling and warming (Fig. 2). Note that the LF forcing also influences the horizontal scale of the cloud and motion of the ice-saturated area (unresolved in our model) at a larger scale. We use a vertical velocity amplitude of $\hat{w}_{\mathrm{LF}} \simeq 0.74$ cm s$^{-1}$, a value derived from the observed temperature fluctuation of $\hat{T}_{\mathrm{LF}} = 4$ K over a period $t_p = 4$ d as described in Cao et al. (2025). This velocity is calculated via $\hat{w}_{\mathrm{LF}} = \omega \hat{T}_{\mathrm{LF}}/\Gamma$, where $\omega = 2\pi/t_p$ is the observed angular frequency and $\Gamma$ is the dry adiabatic lapse rate. In discussing the effects of the LF forcing on TTL cirrus evolution, we distinguish four phase scenarios ($\phi$) corresponding to different sequences of cooling and warming, as shown in Fig. 2. Note here that simulations are initialized at the same temperature, no matter the phase, such that differences arise solely from the phase-dependent thermodynamic evolution imposed by the vertical wind of the wave.

https://doi.org/10.5194/egusphere-2026-3112
Preprint. Discussion started: 10 July 2026


### 2.3 Initialization of the simulations

Thin TTL cirrus with optical depths below 0.002 and cloud bases above 14 km were selected from the full BeCOOL dataset (LATMOS/IPSL, 2024) to constrain our model initial conditions. This subset is characterized by a mean temperature of 192 K at an altitude of about 17 km (100 hPa), with corresponding temperatures from the European Centre for Medium-Range Weather Forecasts reanalysis 5th generation (ERA5) ranging from 185 to 205 K. The observed clouds have a mean vertical extent of 440 m. Mean optical extinction and optical depth are $1.1 \times 10^{-6}$ m$^{-1}$ and $5.2 \times 10^{-4}$, respectively. The mean extinction is used to constrain the initial ice-phase variables in the model.

The model initializes a cirrus layer of depth 200 m at the top of an ice-saturated air column at 192 K. Note that it is larger than typical nucleation layer depths reported in observations (Jensen et al., 2013) and models (Kärcher et al., 2025). This choice assumes that the modeled cirrus layer has already evolved for some time after formation, consistent with the observational sampling.

To constrain the vertical extension of the column $L$ (section 2.1), we assume that the observed cirrus layer depths from the BeCOOL dataset represent the thickness of the corresponding ice-supersaturated columns where ice clouds can be sustained. To account for the observed variability, $L$ is varied across ensemble members. At the start of each simulation, $L$ is drawn from an exponential distribution of cirrus layer depths with a mean of 440 m, consistent with lidar observations (Lesigne et al., 2024). Values of $L$ exceeding 2 km are rejected to omit optically thicker TTL cirrus. Values below 200 m are also rejected as the ice-saturated column contains the cloud layer (see Fig. 1, $L \geq \Delta z$). Although planetary-scale waves might also modulate $L$, current observational constraints are insufficient to represent this effect in our simulations.

At the start of each simulation, $J = 5{,}000$ SIP are initialized at random vertical positions within the cirrus layer and with random radii drawn from a lognormal distribution, characterized by a total number concentration ($n$), mean radius ($\bar{r}$), and a fixed geometric standard deviation of $\sigma_r = 1.5$. Each SIP is assigned a minimum number concentration of $n/J$. The dependence of our results on this initial $\sigma_r$ value is weak. All simulations are terminated, and cirrus lifetimes recorded, when fewer than 100 SIP remain. We run ensembles of 15,000 simulations, sufficient to generate robust cirrus lifetime statistics. We set the time step to 10 s to accurately simulate fast microphysical responses to the wave-induced fluctuations.

The observations do not provide us with information on how the probed cirrus clouds formed or how much time passed since formation, and it is not immediately obvious how to determine initial values of $n$ and $\bar{r}$. Here, we constrain pairs of $\{n, \bar{r}\}$-values using the BeCOOL extinction (E) observations:

$$n = \frac{E}{\int_0^\infty Q_{\mathrm{sca}}(r)\,\pi r^2 \frac{dF}{dr}(r; r_m, \sigma_r)\,dr}, \quad r_m = \bar{r}\exp[-0.5\ln^2(\sigma_r)], \tag{1}$$

with the normalized initial ice crystal number-size distribution, $dF/dr$, and the geometric mean radius, $r_m$. The light scattering efficiency,

$$Q_{\mathrm{sca}} = 2 - \frac{4}{\varrho}\left[\sin(\varrho) - \frac{1-\cos(\varrho)}{\varrho}\right], \quad \varrho = \frac{4\pi r(\mu - 1)}{\lambda}, \tag{2}$$

https://doi.org/10.5194/egusphere-2026-3112
Preprint. Discussion started: 10 July 2026


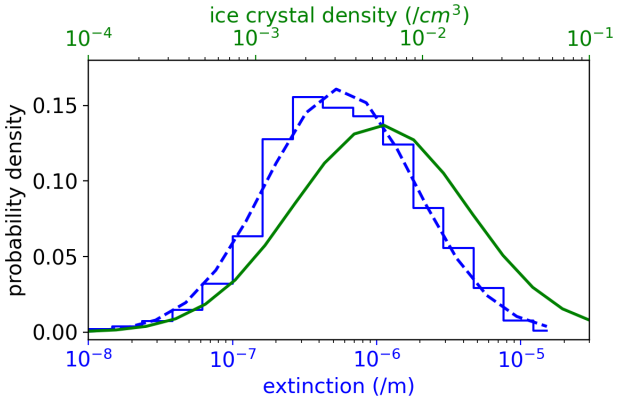


**Figure 3.** Frequency distribution of cirrus extinction from BeCOOL observations (stair steps) and a log-normal fit (dashed blue curve). Frequency distribution of ice crystal number concentrations (green) constrained by the fitted extinction for $\bar{r} = 4\,\mu$m.

is evaluated at the lidar wavelength $\lambda = 0.802\,\mu$m and with the real refractive index for bulk ice, $\mu = 1.311$. Equation 2 approximates the Mie extinction efficiency for non-absorbing spheres of low ($|\mu - 1| \ll 1$) refractive index (van de Hulst, 1981). For large ice crystal sizes in the geometric optics limit, $Q_{\rm sca} \to 2$, so that $n \propto 1/\bar{r}^2$ according to Eq. 1. For crystals much smaller than $\lambda/(2\pi)$, light scattering takes place in the Rayleigh regime with $Q_{\rm sca} \propto r^4$ and therefore $n \propto 1/\bar{r}^6$. The characteristic Mie oscillations due to light scattering are smoothed out by averaging over the size distribution in Eq. 1.

For initialization, we prescribe the mean radius $\bar{r}$, draw an extinction value $E$ from a lognormal fit to the observed extinction statistics, and then derive the corresponding ice crystal number concentration $n$ using Eq. 1. The resulting distributions are shown in Fig. 3, with $\bar{r} = 4$ $\mu$m taken as the baseline initial value. Ice crystals with substantially larger radii settle out of the column quickly, making such cases inconsistent with the long lifetimes observed. Conversely, much smaller radii would represent very young cirrus, but it is unlikely that the lidar observations captured the brief formation stage of the detected clouds. Evaluating Eq. 1 at the mean observed extinction yields $n = 0.009$ cm$^{-3}$. These values of $\bar{r}$ and $n$ are consistent with aircraft measurements of ultra-thin tropical tropopause clouds (Luo et al., 2003) and the associated ice water content is within the range of data sampled in-situ in the coldest parts of the TTL (Thornberry et al., 2017).

We run different scenarios. The baseline scenario (Base) assumes an initial temperature of 192 K and an initial mean ice crystal radius of $4\,\mu$m. Variations in these parameters would affect ice crystal growth rates and, thus, cirrus lifetimes. Therefore, we discuss sensitivity scenarios to assess the effect of such variations relative to Base. Scenarios Temp-184K and Temp-200K use 184 K and 200 K, for temperature excursions of $\pm 8$ K, corresponding to the wave height following Cao et al. (2025). Scenarios Size-2$\mu$m and Size-6$\mu$m prescribe $\pm 2\,\mu$m-variations of $\bar{r}$. These size adjustments, along with the corresponding changes in total ice crystal number concentration, mimic cirrus layers at different stages of evolution, which are not directly constrained by the balloon-borne lidar observations. Finally, as the GW activity (represented in our parameterization with $\sigma_w$) is observed to change geographically, we investigate the effects of different amplitudes of the GW forcing: we prescribe

https://doi.org/10.5194/egusphere-2026-3112
Preprint. Discussion started: 10 July 2026


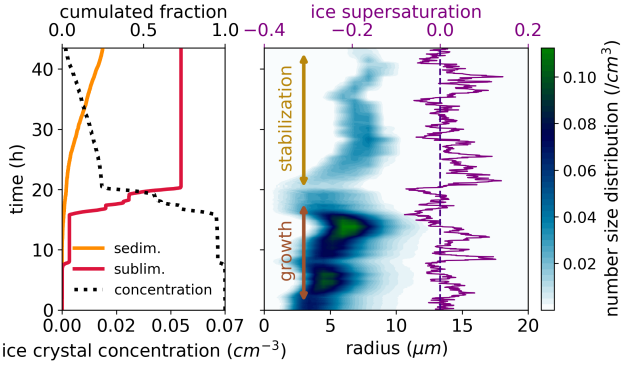


**Figure 4.** Evolution of ice crystal population number-size distribution for a long-lived cloud (right panel) and corresponding total ice crystal concentration and fraction of sedimented and sublimated crystals (left panel).

variations in $\sigma_w$ relative to Base in scenarios Geo-continent and Geo-ocean in line with SPB measurements in continental and oceanic regions.

## 3 Results

We present results from running 15,000 simulations for different scenarios detailed in section 2.3. All scenarios assume an initial cirrus layer at ∼17 km (100 hPa) with a 200 m depth, contained in an initially ice-saturated column forced homogeneously by GW. Scenarios Base is discussed in section 3.1 along with sensitivity tests (scenarios Temp-200K, Temp-184K, Size-2$\mu$m, Size-4$\mu$m, Geo-continent and Geo-ocean). The role of LF forcing in the presence of GW activity is explored in section 3.2.

### 3.1 Influence of gravity waves

#### 3.1.1 Evolution of cloud characteristics

The evolution of ice crystal populations during the cloud lifetime is highly impacted by GW-induced temperature perturbations. Figure 4 describes the evolution of the number-size distribution for an especially long-lived cirrus cloud with a lifetime of 43.5 h in the Base scenario. Warming perturbations ($s' < 0$) lead to a decrease of the mean crystal radius ($\bar{r}$) and a sublimation event that almost dissolved the cloud at around 18 h. Reversely, cooling fluctuations ($s' > 0$) drive deposition growth from initially $\bar{r} = 4$ $\mu$m to about 8 $\mu$m. Although the mean radius increases with time, it remains below 8 $\mu$m on average (see Fig. 5), as sedimentation ultimately limits crystal growth. Ice loss processes respond differently to temperature fluctuations: sublimation occurs in a stepwise manner tied to warming events, whereas sedimentation increases more steadily with cooling and growth.

Figure 4 highlights two different regimes: the growth phase is characterized by an overall net supersaturation, and ice crystals growth to reach a size for which full sublimation due to GW temperature fluctuations is less likely to occur. Note that the full sublimation tends to happen early, when ice crystals are still small and thus more sensitive to warming events, as sublimation

https://doi.org/10.5194/egusphere-2026-3112
Preprint. Discussion started: 10 July 2026


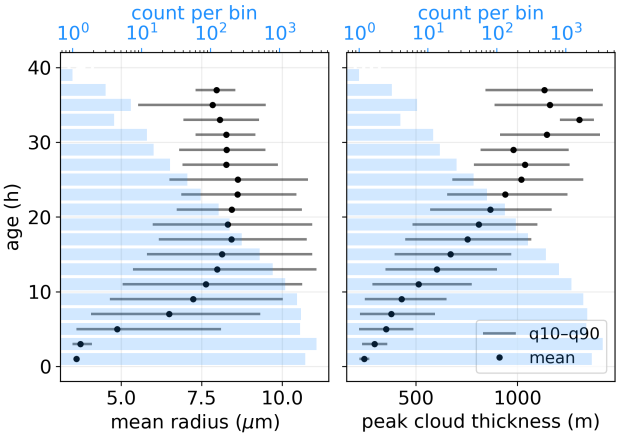


**Figure 5.** Evolution of mean radius (left panel) and peak cloud thickness (right panel) with cloud age. Data counts per bin are represented by background histograms. q10 and q90 represent 10 % and 90 % quantiles, respectively.

rates rapidly increase with decreasing crystal radii. A warming event is then less likely to dissolve the cloud once ice crystals are big enough: this is the stabilization regime (Fig. 4). During the stabilization regime, thin TTL cirrus can be sustained with a sequence of rapid GW-induced warming and cooling events. In this stage of cloud evolution, amplitudes of warming perturbations rarely become large enough to sublimate the entire crystal population but prevent significant net deposition growth and a fast sedimentation of ice crystals, as shown in Fig. 4. This cloud dissipates by slow sedimentation of the ice crystals out of the column. Our simulations thus reveal an interesting stabilization mechanism that happens in the presence of GW activity, and that prolongs TTL cirrus lifetimes in the absence of slow, large-scale temperature variations.

GW-driven temperature perturbations affect both ice crystal microphysics and cloud thickness, the latter evolving in time through sedimentation. As shown in Fig. 5, cloud thickness increases with age. This thickening is linked to a broadening of the size distribution: ice crystals large enough to survive warming events sediment and coexist with smaller ones that remain within the initial cloud layer. Such diversity in the crystal population helps explain why some clouds achieve longer lifetimes. This behavior is consistent with the stabilization effect noted above and is reflected in the evolution of the mean radius (Fig. 5). In the binned statistics, a transition toward this regime emerges around 4–6 h. At this stage, clouds that persist exhibit broader size distributions, which shifts towards bigger sizes as smaller crystals are preferentially removed during early warming events while larger ones survive and grow. This apparent transition reflects the typical timescale over which ice crystals either grow to sizes resistant to sublimation or are removed by early fluctuations. While the timing varies across individual realizations and depends on the sequence of cooling and warming events, stabilization becomes increasingly likely once crystals have grown sufficiently for complete sublimation to be unlikely. This transition therefore marks a key stage in cirrus evolution, separating short-lived clouds from those able to enter a long-lived stabilization regime.

https://doi.org/10.5194/egusphere-2026-3112
Preprint. Discussion started: 10 July 2026


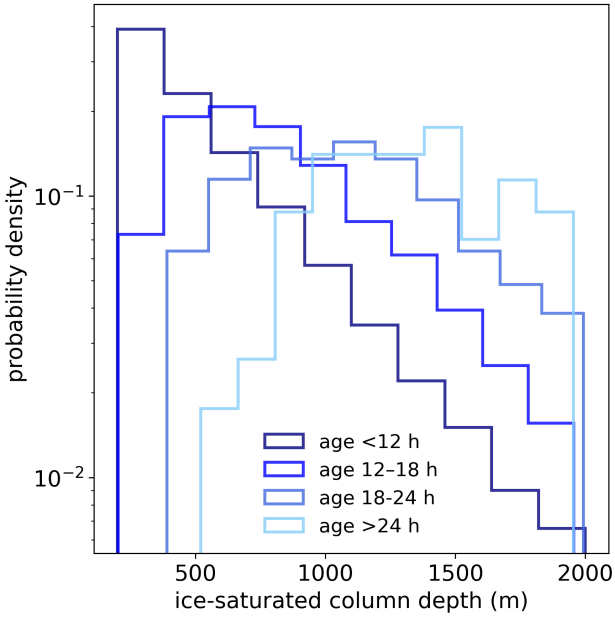


**Figure 6.** Probability distributions of depths of ice-saturated columns for cirrus clouds of different cumulated age bins.

### 3.1.2 Sensitivity to environment and initial conditions

#### Depth of ice-saturated columns

We recall that the depth of the ice-saturated column ($L$) is drawn from a truncated exponential probability distribution and is set as an initial condition (section 2.3). A thicker column allows sedimenting ice crystals to persist longer and thus enhance cloud lifetime. This is illustrated in Fig. 6 where long-lived (>12 h) cirrus are associated with deeper layers, indicating the role of initial environmental conditions in sustaining TTL cirrus for long durations. Conversely, short-lived cirrus exhibit distributions of $L$ similar to the initialized distribution. Together, this means that the influence of $L$ emerges only once ice crystals have had sufficient time to grow and sediment out. This result is also supported by Fig. 7: short-lived clouds are exclusively terminated by sublimation, and their lifetimes are controlled by the sequence of warming and cooling events associated with GW activity, showing little dependence on $L$. In contrast, longer-lived cirrus exhibit a clear correlation between lifetime and $L$. Our results indicate that the longest-lived cirrus clouds occur only in sufficiently deep ice-saturated layers.

#### Temperature and mean ice crystal radius

The sensitivity to environmental temperature is evaluated in scenarios Temp-184K and Temp-200K. In a colder environment, the ice crystal population does not grow to radii as large as in Base (Fig. 8) due to lower deposition growth rates and a smaller amount of water vapor available for ice growth. At the same time, sublimation rates are smaller, reducing the impact of GW-

https://doi.org/10.5194/egusphere-2026-3112
Preprint. Discussion started: 10 July 2026


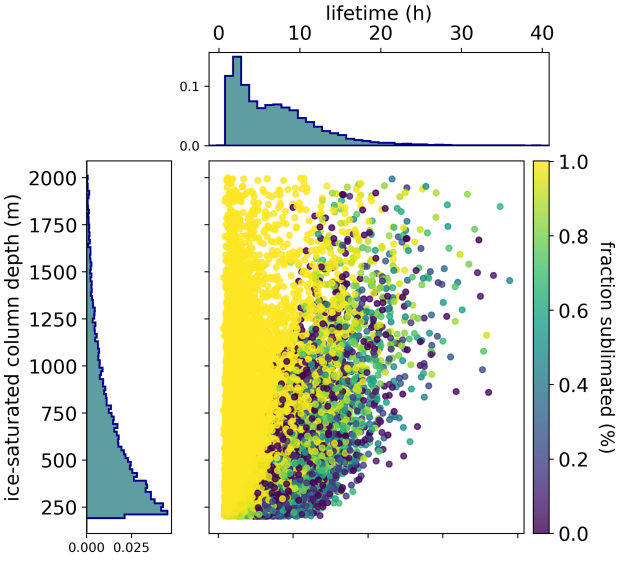


**Figure 7.** Probability distributions of lifetime and ice-saturated column depth (outer panels); the scatter plot (main panel) marks joint values colored by fraction of fully sublimated ice crystals.

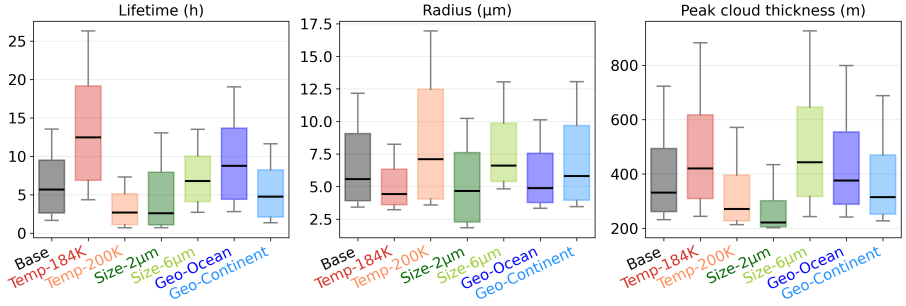


**Figure 8.** Boxplots of lifetime, radius and peak cloud thickness for the Base, Temp, Size and Geo scenarios. Averages are represented as thick horizontal lines and whiskers extend from 10 % to 90 % quantiles.

induced warming events and allowing ice crystals to persist longer. Besides, initial sizes might be large enough to survive warm excursions at lower temperatures. Consequently, lower temperatures yield cirrus clouds with lifetimes roughly twice as long as those in scenario Base. In contrast, ice crystals in a warmer environment reach larger mean sizes than in the Base scenario. The average lifetime of such clouds is only half as long, as enhanced sublimation during warming phases and faster sedimentation of larger crystals favor cloud dissipation, leading to a smaller mean cloud depth than in the 184 K case and scenario Base.

The sensitivity of simulated cirrus lifetimes to the initial mean ice crystal radius is assessed with the help of scenario Size (Fig. 8). Smaller ice crystal populations ($\bar{r} = 2$ $\mu$m) are more susceptible to GW-induced warming events, leading to enhanced sublimation and, consequently, shorter lifetimes on average and geometrically thinner clouds. In contrast, clouds with initially

https://doi.org/10.5194/egusphere-2026-3112
Preprint. Discussion started: 10 July 2026


larger crystals ($\bar{r} = 6$ $\mu$m) are less frequently terminated by sublimation, resulting in an increased average lifetime. In these simulations, a greater fraction of the ice crystal population is lost by sedimentation rather than sublimation. Interestingly, lifetime distributions is more skewed towards longer times for the $\bar{r} = 2$ $\mu$m case than the $\bar{r} = 6$ $\mu$m case. For a few occurrences, some crystals reach the stabilization regime with an optimal size range to not fully sublimate nor rapidly sediment, enabling very long lifetimes.

**Gravity wave forcing variability**

Tropical GW activity exhibits pronounced regional variability linked to deep convection in the troposphere (Alcala and Dessler, 2002). Observations indicate that oceanic regions are generally quiescent, whereas continents and the Maritime Continent experience stronger GW momentum fluxes and enhanced vertical wind variability (Wright et al., 2013; Corcos et al., 2021; Randel et al., 2021; Corcos et al., 2025). To account for this contrast, scenarios Geo-ocean and Geo-continent prescribe different forcing amplitudes representative of oceanic ($\sigma_w = 6$ cm.s$^{-1}$) and continental ($\sigma_w = 16$ cm.s$^{-1}$) environments.

Across all imposed dynamical regimes in scenarios Base and Geo, sublimation losses remain more likely than sedimentation losses. Pure sedimentation cases are rare (<5%), while the probability of complete sublimation increases with increasing $\sigma_w$, rising from about 18% to 21% between oceanic and continental conditions. In contrast, weaker perturbations produce flatter distributions of sublimated and sedimented fractions, as they cause fewer intense warming events capable of terminating clouds, and fewer strong cooling phases that would otherwise promote rapid growth.

The stabilization regime also depends on wave activity. The quasi-equilibrium mean radius increases from about 5 $\mu$m in oceanic conditions to $\sim 6$ $\mu$m in continental conditions (Fig. 8), indicating that stronger dynamical forcing requires larger crystal sizes for survival against frequent sublimation events of larger amplitude. This sensitivity can be illustrated using the sublimation timescale estimate derived in Appendix B. Under typical tropical tropopause conditions (192 K, 100 hPa), small ice crystals ($\sim 5$ $\mu$m) can be rapidly removed by warming rates of order 6–7 K h$^{-1}$, corresponding to GW-driven downdrafts of $\sim 20$ cm.s$^{-1}$. Such events are relatively frequent, with probabilities increasing from a few percent in oceanic conditions to about 30% in continental regions (Appendix B). Larger crystals in the stabilization regime are significantly more resilient: for a given warming event, they require either stronger or more persistent subsaturation to fully sublimate and therefore survive a larger fraction of fluctuations. As a result, the probability of complete sublimation decreases with increasing crystal size, even though stronger GW activity enhances the occurrence of intense warming events for all sizes. Our results show that cirrus lifetime is thus controlled by the high-amplitude tail of the vertical wind distribution rather than its mean value. Stronger GW activity increases the frequency of these extreme events while simultaneously shifting the stabilization regime toward larger crystal sizes, thereby shortening cirrus lifetimes overall.

### 3.2 Role of the low frequency wave forcing

The inclusion of LF wave forcing introduces a pronounced phase-dependent modulation of cirrus evolution by shifting the balance between depositional growth, sedimentation, and sublimation (Fig. 9). In the absence of GW, the LF wave imposes a deterministic evolution, depending on the wave period and amplitude. We recall here that all simulations start with the same

https://doi.org/10.5194/egusphere-2026-3112
Preprint. Discussion started: 10 July 2026


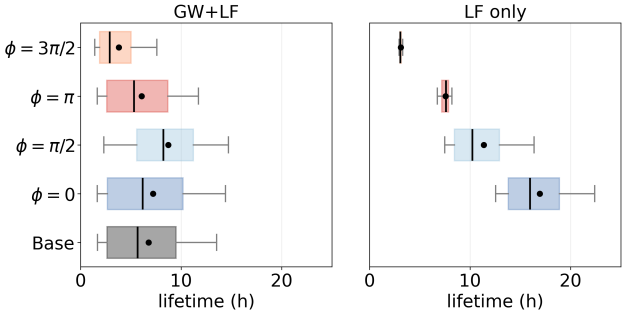


**Figure 9.** Boxplots of cirrus lifetimes for the scenario Base and for the four LF phases mixed with gravity waves (left panel) and LF forcing only (left panel). The average is a straight line and the median is a dot. Whiskers extend from 10% to 90% quantiles.

| | LF phase | 0 | $\pi/2$ | $\pi$ | $3\pi/2$ |
|---|---|---|---|---|---|
| fraction (%) of ice crystals sublimated | GW+LF | 71 (98) | 43 (27) | 84 (99) | 95 (100) |
| mean (median) | LF | 0 (0) | 0 (0) | 97 (99) | 99 (100) |

**Table 1.** Fraction of sublimated crystals for simulations only using LF, and simulations combining GW and LF forcings. Note that the fraction of sedimented crystals can be inferred from 100%-fraction sublimated.

initial temperature of 192 K, irrespective of the phase, and differ only by the evolution of vertical wind. For a 4 day period, clouds initialized in the cooling part of the wave ($\phi = 0$ and $\phi = \pi/2$) can persist until complete sedimentation, with almost no sublimation losses, as the cloud mostly dissipates before the warming phase of the wave. Reversely, clouds initialized in the warming part ($\phi = \pi$ and $\phi = 3\pi/2$) are rapidly depleted by sublimation (Table 1). This binary behavior reflects the slowly varying thermodynamic tendency imposed by the LF wave alone. Note that the variability of lifetimes for each phase (Fig. 9) depends solely on the $L$. Cooling phases exhibit more variability as sedimentation of ice crystals make $L$ a limiting factor of cloud lifetime. Reversely, sublimation of ice crystals does not depend on $L$.

Adding GW substantially modifies this picture. High-frequency temperature fluctuations broaden the lifetime distributions and introduce intermittent sublimation events even during LF cooling phases. Indeed, for $\phi = 0$, the effect of the initially weak cooling (see Fig. 2) is easily balanced by the GW higher amplitude warming events, resulting in a substantial shortening of the cloud lifetime. For $\phi = \pi/2$, initial larger LF cooling sustained for hours promotes depositional growth, allowing ice crystals to reach larger radii and enter the stabilization regime, which produces the longest lifetimes on average for simulations with LF and GW. However, GW-induced warming events still remove a fraction of the ice population, increasing the mean sublimated fraction relative to the LF-only case (Table 1). In contrast, the LF warming phases maintain subsaturated conditions and favor small crystal sizes. In these conditions, the GW fluctuations widen the distribution of lifetimes: GW warming fluctuations are enhanced, and clouds can dissipate rapidly, with nearly all crystals lost by sublimation, resulting in shorter lifetimes. At the same time, the GW cooling and warming fluctuations can help reaching a stabilization in size of the ice crystals, which enhances the lifetime of the cirrus clouds. Overall, the LF wave sets the large-scale thermodynamic pathway, while GW shift

https://doi.org/10.5194/egusphere-2026-3112
Preprint. Discussion started: 10 July 2026


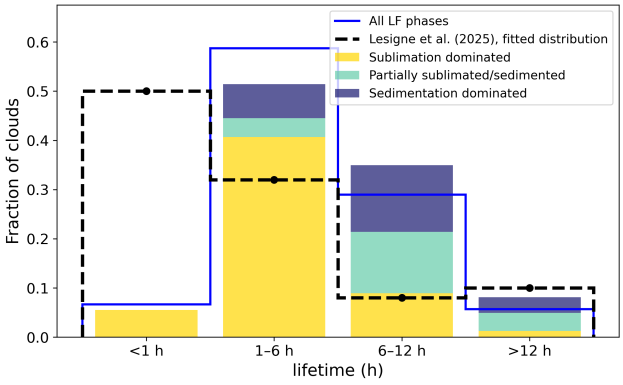


**Figure 10.** Distribution of simulated cirrus lifetimes compared to the fitted lifetime distribution from Lesigne et al. (2025). Colored bars show the fraction of clouds dominated (>90% of crystals) by sublimation, sedimentation, or a combination of both processes for simulations including only a cooling phase of LF wave. The dashed black line represents the fitted observational distribution. The blue line shows the lifetime distribution obtained when all LF wave phases are included.

| Lifetime range | <1h | 1-6h | 6-12h | >12h |
|---|---|---|---|---|
| Cloud fraction (%) | 7 (5) [*50*] | 59 (52) [*32*] | 29 (35) [*8*] | 6 (8) [*10*] |
| Cloud coverage (%) | 1 (1) [*3*] | 34 (27) [*15*] | 48 (50) [*12*] | 17 (22) [*71*] |

**Table 2.** Fraction of simulated cirrus clouds and associated integrated cloud coverage as defined in Lesigne et al. (2025) for different lifetime ranges. Values outside the parentheses correspond to simulations including all LF wave phases randomized, while values in parentheses correspond to simulations with LF cooling phases only. Values in square brackets correspond to Lesigne et al. (2025) study.

the lifetime through large amplitude sublimation or intermittent cooling. The results highlight a LF phase dependence, which is consistent with previous observational and modeling studies showing that tropical cirrus preferentially form and persist within wave-driven cold anomalies (Kim et al., 2016), while warming phases reduce supersaturation and promote cloud dissipation (Podglajen et al., 2018).

## 4 Comparison with micro-lidar observations

For a first-order comparison with Lesigne et al. (2025), we compare our simulated lifetime statistics obtained with the GW forcing and a LF wave phase randomly sampled between 0 and $\pi$ (corresponding to the cooling phase), to the fitted distribution of apparent cloud lifetimes inferred from BeCOOL observations (Fig. 10). TTL cirrus are preferentially observed within wave-driven cold anomalies (Lesigne et al., 2024), and since the LF phase of individual observed clouds is not constrained, this choice should be viewed as a physically motivated sampling assumption rather than a direct observational constraint.

Both distributions exhibit an asymmetry, characterized by a larger fraction of short-lived clouds (lifetime $< 6$ h) and a smaller population of long-lived cirrus. In particular, the simulations reproduce a key feature of the BeCOOL observations: clouds with

https://doi.org/10.5194/egusphere-2026-3112
Preprint. Discussion started: 10 July 2026


lifetimes exceeding 12 h represent a non-negligible fraction of occurrences (∼6–10%) but contribute disproportionately to total cloud coverage (Table 2). In the simulations, cirrus with lifetimes longer than 12 h account for only 6% (8%) of clouds but 17% (22%) of the integrated cloud coverage when considering all LF phases (cooling phases only). This result is consistent with the observational interpretation that long-lived cirrus, although rare, may dominate the radiative impact (Lesigne et al., 2025).

The model produces fewer very short-lived clouds ($< 1$ h) and a larger fraction of intermediate lifetimes (1–12 h) compared to the fitted observational distribution. In particular, the BeCOOL observations were collected over tropical oceans, where gravity-wave activity is generally weaker than in continental regions. Simulations representative of oceanic conditions (Geo-ocean) yield even longer lifetimes and a larger fraction of long-lived cirrus than the Base configuration, increasing the discrepancy with the observational distribution. Still, the agreement between simulated and observed lifetime statistics is encouraging given the sensitivity of cirrus evolution to both the initial cloud properties and the dynamical environment. Several factors may contribute to these differences. Our model considers a single idealized LF wave, whereas observed cirrus may evolve under the influence of multiple interacting tropical wave modes. In addition, ice nucleation is not explicitly represented and the simulations focus on the evolution of pre-existing cirrus layers rather than rapidly forming and dissipating clouds. Neither observations nor simulations constrain the cloud age at the time of detection or initialization, introducing an unknown lifetime offset that primarily affects clouds in the shortest lifetime category. Finally, the observational lifetimes derived by Lesigne et al. (2025) correspond to balloon-following apparent lifetimes rather than purely Lagrangian cloud evolution. Given these uncertainties, the overall agreement in the shape of the lifetime distribution and in the fraction of long-lived clouds should be regarded as robust support for the proposed physical interpretation.

Simulations including LF phases randomly sampled between 0 and $2\pi$ (Fig. 10) yield similar overall statistics, with differences mainly affecting the longest-lived clouds. Restricting the sampling to cooling phases increases the fraction of cirrus able to survive beyond 6–12 h, consistent with the preferential occurrence of TTL cirrus within cold anomalies.

Beyond the overall agreement of our results with the observations, the process-based nature of our model provides a physical interpretation of the observed lifetime distribution. Short-lived clouds are almost exclusively terminated by sublimation, whereas longer-lived cirrus emerge once ice crystals grow large enough to become less sensitive to warming-induced sublimation. In this stabilization regime, sedimentation becomes the dominant loss process, while intermediate lifetimes correspond to a transition where both mechanisms contribute. The skewed lifetime distribution therefore arises from the competition between sublimation and sedimentation under intermittent dynamical forcing, highlighting the key role of microphysical growth in enabling cirrus persistence.

## 5 Summary and discussion

We investigated how multiscale wave-driven variability controls the persistence of thin TTL cirrus using a process-based Lagrangian microphysical model initialized from BeCOOL lidar observations. The simulations show that cirrus lifetime emerges from the competition between sublimation and sedimentation under fluctuating dynamical forcing.

https://doi.org/10.5194/egusphere-2026-3112
Preprint. Discussion started: 10 July 2026


- Gravity waves influence cirrus evolution through two distinct effects. Moderate cooling and warming fluctuations regulate crystal growth and help create and maintain a stabilization regime in which crystals remain large enough to resist complete sublimation while avoiding significant sedimentation losses. In this regime, cirrus can persist for many hours through a balance between gradual sedimentation and intermittent sublimation. However, the cloud lifetime is ultimately controlled by the rare high-amplitude warming events at the tail of the GW driven fluctuation distribution. These extreme fluctuations can fully sublimate the ice crystal population and abruptly terminate the cloud. As a result, cirrus persistence depends more strongly on the probability of extreme warming excursions than on the mean amplitude of the GW forcing itself.

- LF waves modulate the cloud lifetime by setting the slowly evolving temperature background. Cooling phases promote depositional growth, lower the critical crystal size required to survive GW warming events, and favor long-lived cirrus. In contrast, warming phases enhance the probability of rapid cloud dissipation. Simulations including LF forcing only reveal a strongly phase-dependent behavior: clouds initialized during warming phases are almost entirely removed by sublimation, whereas clouds initialized during cooling phases can persist long enough for sedimentation to become important. Only the addition of GW variability changes this deterministic evolution and produces lifetime distributions broader and closer to observations.

- The simulated lifetime statistics reproduce the strongly skewed distribution inferred from BeCOOL observations, including a small but climatically important population of long-lived cirrus. Indeed, although clouds persisting longer than 12 h represent only a small fraction of occurrences, they contribute disproportionately to the cloud coverage and likely dominate the cumulative radiative impact of thin TTL cirrus.

Several limitations of our method should be noted. Ice nucleation is not explicitly represented, as simulations assume pre-existing cirrus in an initially ice-saturated environment, for which GW–induced variability alone is generally insufficient to trigger new nucleation events. Introducing a low-frequency wave of larger amplitude can, however, drive the background conditions toward higher supersaturation levels. Depending on the assumed homogeneous freezing threshold, these conditions are met up to $\sim$2% of the time for $S_i = 1.9$ and $\sim$7% for $S_i = 1.6$ in the cold phase of the LF wave. These values span the range of thresholds commonly assumed (Koop et al., 2000) and in TTL conditions. As a result, sporadic in situ nucleation may contribute to cirrus maintenance in reality and the simulated lifetimes should be viewed as a lower bound. More generally, cirrus formation is prescribed through observation-constrained initial conditions, with a pre-existing ice crystal population. Results using only the LF wave forcing would be drastically different if the initialization of the simulations would have been driven by homogeneous nucleation from the LF wave cooling for example.

In addition, the model assumes a vertically homogeneous thermodynamic structure, whereas atmospheric waves can generate vertical variability that may expose settling crystals to different saturation conditions. However, this effect is likely limited given that the prescribed saturated layer depth is consistent with typical fractions of GW vertical wavelengths reported in observations.

https://doi.org/10.5194/egusphere-2026-3112
Preprint. Discussion started: 10 July 2026


Future work combining process-based simulations with long-duration Lagrangian observations and the inclusion of nucleation will help further constrain the mechanisms controlling TTL cirrus persistence and their climate impact.

*Data availability.* The BeCOOL retrieved extinction profiles (Level 2 data) are available from the IPSL Data Catalog (https://doi.org/10.14768/bad47567-f844-4084-abd9-917668e18d82). Supplementary dataset with BeCOOL cloud top and base altitudes and optical depths are available at https://doi.org/10.5281/zenodo.20323595.

## Appendix A: Estimation of cirrus radiative heating

Radiative heating within cirrus can drive convective motions to mesoscale circulations (Dinh et al., 2023). We estimate air temperature tendencies (cloud radiative heating, CRH) due to thin TTL cirrus as represented in our numerical simulations to judge the potential importance of cloud-radiation interactions. The change in radiative fluxes in the shortwave (SW) and longwave (LW) spectral region due to the presence of cloud and relative to the unperturbed atmosphere (without cloud) is called cloud radiative effect (CRE). CRH follows from the energy balance for the cloudy layer: CRH = CRE/($c_p \rho_a \Delta z$), with the specific heat capacity of air at constant pressure, $c_p$, and the mass density of air, $\rho_a$.

For optically thin and cold cirrus, the cooling SW CRE (< 0) is typically smaller than the warming LW CRE (> 0). We estimate in a first step an upper limit CRH from LW CRE alone. In a second step, we estimate an average tropical SW CRE using a parametric radiative transfer model to determine net diabatic temperature changes due to CRH. The net LW CRE is given by $\sigma_{\mathrm{SB}}(T_{\mathrm{b}}^4 - T^4)$, with the Stefan-Boltzmann constant $\sigma_{\mathrm{SB}}$ and the cloud temperature $T$ (Liou et al., 1990). The brightness temperature ($T_{\mathrm{b}}$) characterizes the radiation flux without the cirrus layer. The emissivity, $\epsilon = 1 - \exp(-0.468\,\mathrm{COD}^{0.988})$, is included since cirrus do not act as black bodies. We evaluate $\epsilon$ at the highest optical depth of the subset of BeCOOL thin cirrus clouds (0.002) to maximize the radiative effect. Values $T_{\mathrm{b}} = 260 - 280$ K approximately bounding measurement conditions give ranges of CRE = $0.18 - 0.27$ W m$^{-2}$ and CRH = $0.2 - 0.29$ K d$^{-1}$ for pure LW forcing, respectively.

The semi-quantitative parameterization developed by Corti and Peter (2009) has been tested against a state-of-the art radiative transfer scheme and was judged useful for first-order estimates of top-of-the-atmosphere cirrus cloud forcing (Lolli et al., 2017). It predicts LW CRE in good agreement with our estimate, as well as a diurnally averaged SW CRE of $-0.2$ W m$^{-2}$ for tropical insolation. Taken together, our estimated net CRH and equivalent updraft speed for the BeCOOL case study are < 0.08 K d$^{-1}$ and < 0.09 mm s$^{-1}$, much smaller than the mean net diabatic heating rate and associated large-scale upwelling at the tropical tropopause. Because the wave-induced vertical wind speed fluctuations used in this study are much larger, it is justified to neglect radiatively induced temperature changes.

## Appendix B: Estimation of sublimation timescales

We estimate sublimation times of ice crystals with initial radius $r$ for a given GW-induced vertical wind speed fluctuation $w'$. Our calculation is based on the single particle growth law describing diffusional uptake of water vapor on spherical ice crystals

https://doi.org/10.5194/egusphere-2026-3112
Preprint. Discussion started: 10 July 2026


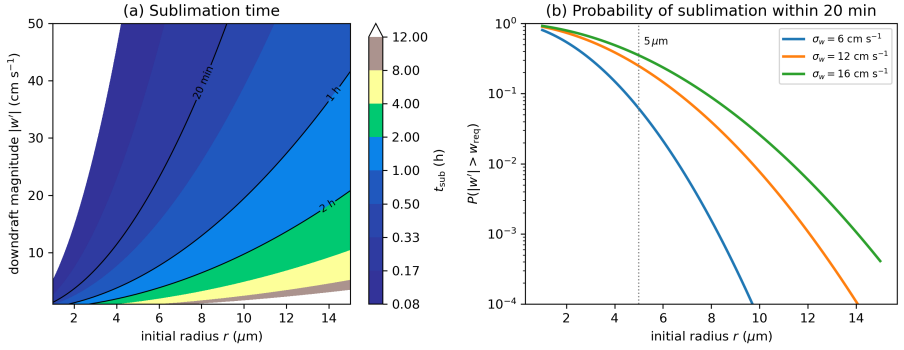


**Figure B1.** Estimated sublimation timescales of spherical ice crystals under gravity-wave-induced warming events for typical conditions at the cold point tropopause (192 K, 100 hPa). (a) Sublimation time as a function of downdraft magnitude for several initial crystal radii. Small crystals can be fully sublimated within minutes under strong warming events, whereas larger crystals are substantially more resistant. (b) Probability that the downdraft required for complete sublimation occurs for exponential gravity-wave vertical velocity distributions representative of oceanic (blue), Base (orange), and continental (green) conditions. The rapid decrease in probability with increasing crystal radius illustrates why larger crystals are less sensitive to complete sublimation and why the high-amplitude tail of the gravity-wave distribution controls cirrus persistence.

with a kinetic correction that interpolates the molecular flux of water vapor from the gas phase in the far field of the particle towards its surface (Lamb, D., & Verlinde, J., 2011):

$$\frac{dr}{dt} = \frac{\beta(r)}{r} G\, s', \quad G = vDn_{\mathrm{sat}}, \quad \beta \simeq \left(1 + \frac{\ell}{\alpha r}\right)^{-1}, \tag{B1}$$

with the characteristic diffusional growth factor $G$ per unit supersaturation and the molecular volume water in bulk ice ($v$), the diffusion coefficient of water molecules in air ($D$), the number concentration of water molecules in air at ice saturation ($n_{\mathrm{sat}}$), and the kinetic correction factor ($\beta$) with the diffusion length scale ($\ell$) and the sublimation coefficient ($\alpha$). In TTL conditions, $\ell \approx 0.9\,\mu$m and setting $\alpha = 1$ implies that sublimation is not hindered by molecular processes at ice crystal surfaces (Nelson and Baker, 1996). Effects of latent heat and ventilation are not included in Eq. (B1), as they do not significantly affect $dr/dt$.

To relate $w'$ to supersaturation fluctuations $s'$ due to GW forcing, we make use of the relationship $|s'| = \Gamma |w'| \kappa/\nu$ (Kärcher and Podglajen, 2019), where $\Gamma$ is the dry adiabatic lapse rate, $\kappa$ is a thermodynamic factor ($\approx 0.15$), and $\nu = 3.5\ \mathrm{h}^{-1}$ is a characteristic GW frequency converting temperature to cooling/heating rate fluctuations in line with continuous SPB measurements within $\pm 15°$ latitude.

Equation (B1) yields the sublimation time

$$t_{\mathrm{sub}} = \frac{1}{G|s'|} \int_{r_c}^{r} \frac{r}{\beta(r)} dr, \tag{B2}$$

where $r_c = 0.1\ \mu$m is the radius of the dry aerosol core released by a fully sublimated ice crystal. We solve the integral for constant $w'$ and neglect corresponding changes in air temperature and pressure, hence $s'$, during the sublimation event.

https://doi.org/10.5194/egusphere-2026-3112
Preprint. Discussion started: 10 July 2026


In nature $s'$ may relax towards zero during the sublimation event. Our approach to estimate sublimation times is therefore valid if the subsaturation quenching timescale ($t_{\mathrm{q}}$) exceeds $t_{\mathrm{sub}}$. This is justified by the rather high GW-induced cerical wind speed fluctuations and typically low number concentration and small size of ice crystals in TTL cirrus. Evaluating $t_{\mathrm{q}} = 1/(4\pi D\beta nr)$ (Korolev and Mazin, 2003) shows that $t_{\mathrm{q}} > t_{\mathrm{sub}}$ for $|w'| > 12$ cm s$^{-1}$, $r < 5$ $\mu$m and $n < 0.1$ cm$^{-3}$.

Figure B1 illustrates sublimation times and probability of sublimation. Sublimation times increase strongly with crystal radius, implying that progressively stronger warming events are required to completely remove larger crystals (Fig. B1a). Consequently, the probability of complete sublimation decreases rapidly with radius (Fig. B1b). While small crystals are more sensitive to warming fluctuations from GW, larger crystals become increasingly resilient and are more likely to sediment than sublimate. Cirrus lifetime is therefore controlled by the competition between gradual crystal growth toward this stabilization regime and the rare high-amplitude warming events associated with the tail of the gravity-wave distribution.

*Author contributions.* MC and BK conceived the study. MC performed the study with scientific support from BK. MC wrote the paper with contributions from BK, TL, AP and EJ. All authors agreed on the final version.

*Competing interests.* One of the (co-)authors is a member of the editorial board of Atmospheric Chemistry and Physics.

*Acknowledgements.* Milena Corcos was supported by NSF grant number 2231667, the BeCOOL data set was collected as part of Strateole-2, which was sponsored by CNES, CNRS/INSU and NSF.

https://doi.org/10.5194/egusphere-2026-3112
Preprint. Discussion started: 10 July 2026


## References

Alcala, C. M. and Dessler, A. E.: Observations of deep convection in the tropics using the Tropical Rainfall Measuring Mission (TRMM) precipitation radar, J. Geophys. Res., 107, 17–1–17–7, https://doi.org/10.1029/2002JD002457, 2002.

Boehm, M. T. and Verlinde, J.: Stratospheric influence on upper tropospheric tropical cirrus, Geophys. Res. Lett., 27, 3209–3212, https://doi.org/10.1029/2000gl011678, 2000.

Cao, B., Alexander, M. J., Haase, J. S., Corcos, M., and Lesigne, T., R. F.: Characterization of short-vertical wavelength tropical waves shaping cirrus clouds using stratospheric balloon-borne observations, J. Geophys. Res., in review, 2025.

Corcos, M., Hertzog, A., Plougonven, R., and Podglajen, A.: Observation of Gravity Waves at the Tropical Tropopause Using Superpressure Balloons, J. Geophys. Res., 126, https://doi.org/10.1029/2021jd035165, 2021.

Corcos, M., Hertzog, A., Plougonven, R., and Podglajen, A.: A simple model to assess the impact of gravity waves on ice-crystal populations in the tropical tropopause layer, Atmos. Chem. Phys., 23, 6923–6939, https://doi.org/10.5194/acp-23-6923-2023, 2023.

Corcos, M., Bramberger, M., Alexander, M. J., Hertzog, A., Liu, C., and Wright, C.: Observation of Gravity Waves Generated by Convection and the "Moving Mountain" Mechanism During Stratéole-2 Campaigns and Their Impact on the QBO, Journal of Geophysical Research: Atmospheres, 130, https://doi.org/10.1029/2024jd041804, 2025.

Corti, T. and Peter, T.: A simple model for cloud radiative forcing, Atmos. Chem. Phys., 9, 5751–5758, https://doi.org/10.5194/acp-9-5751-2009, 2009.

Dessler, A. E., Palm, S. P., Hart, W. D., and Spinhirne, J. D.: Tropopause-level thin cirrus coverage revealed by ICESat/Geoscience Laser Altimeter System, J. Geophys. Res., 111, https://doi.org/10.1029/2005jd006586, 2006.

Dinh, T. and Fueglistaler, S.: Microphysical, radiative, and dynamical impacts of thin cirrus clouds on humidity in the tropical tropopause layer and lower stratosphere, Geophys. Res. Lett., 41, 6949–6955, https://doi.org/10.1002/2014gl061289, 2014.

Dinh, T., Podglajen, A., Hertzog, A., Legras, B., and Plougonven, R.: Effect of gravity wave temperature fluctuations on homogeneous ice nucleation in the tropical tropopause layer., Atmos. Chem. Phys., 16, 35–46, https://doi.org/10.5194/acp-16-35-2016, 2016.

Dinh, T., Gasparini, B., and Bellon, G.: Clouds and Radiatively Induced Circulations, https://doi.org/10.1002/9781119700357.ch11, 2023.

Dinh, T. P., Durran, D. R., and Ackerman, T. P.: Maintenance of tropical tropopause layer cirrus, J. Geophys. Res., 115, https://doi.org/10.1029/2009jd012735, 2010.

Gasparini, B., Atlas, R., Voigt, A., Krämer, M., and Blossey, P. N.: Tropical cirrus evolution in a kilometer-scale model with improved ice microphysics, Atmos. Chem. Phys., 25, https://doi.org/10.5194/acp-25-9957-2025, 2025.

Hoyle, C. R., Luo, B. P., and Peter, T.: The Origin of High Ice Crystal Number Densities in Cirrus Clouds, J. Atmos. Sci., 62, 2568–2579, https://doi.org/10.1175/jas3487.1, 2005.

Immler, F., Krüger, K., Fujiwara, M., Verver, G., Rex, M., and Schrems, O.: Correlation between equatorial Kelvin waves and the occurrence of extremely thin ice clouds at the tropical tropopause, Atmos. Chem. Phys., 8, 4019–4026, https://doi.org/10.5194/acp-8-4019-2008, 2008.

Jensen, E. J. and Pfister, L.: Transport and freeze-drying in the tropical tropopause layer, J. Geophys. Res., 109, https://doi.org/10.1029/2003jd004022, 2004.

Jensen, E. J., Toon, O. B., Pfister, L., and Selkirk, H. B.: Dehydration of the upper troposphere and lower stratosphere by subvisible cirrus clouds near the tropical tropopause, Geophys. Res. Lett., 23, 825–828, https://doi.org/10.1029/96gl00722, 1996.

https://doi.org/10.5194/egusphere-2026-3112
Preprint. Discussion started: 10 July 2026


Jensen, E. J., Read, W. G., Mergenthaler, J., Sandor, B. J., Pfister, L., and Tabazadeh, A.: High humidities and subvisible cirrus near the tropical tropopause, Geophys. Res. Lett., 26, 2347–2350, https://doi.org/10.1029/1999gl900266, 1999.

Jensen, E. J., Pfister, L., and Toon, O. B.: Impact of radiative heating, wind shear, temperature variability, and microphysical processes on the structure and evolution of thin cirrus in the tropical tropopause layer, J. Geophys. Res., 116, https://doi.org/10.1029/2010jd015417, 2011.

Jensen, E. J., Pfister, L., and Bui, T. P.: Physical processes controlling ice concentrations in cold cirrus near the tropical tropopause, J. Geophys. Res., 117, https://doi.org/https://doi.org/10.1029/2011JD017319, 2012.

Jensen, E. J., Lawson, R. P., Bergman, J. W., Pfister, L., Bui, T. P., and Schmitt, C. G.: Physical processes controlling ice concentrations in synoptically forced, midlatitude cirrus, J. Geophys. Res., 118, 5348–5360, https://doi.org/10.1002/jgrd.50421, 2013.

Jensen, E. J., Ueyama, R., Pfister, L., Bui, T. V., Alexander, M. J., Podglajen, A., Hertzog, A., Woods, S., Lawson, R. P., Kim, J.-E., and Schoeberl, M. R.: High-frequency gravity waves and homogeneous ice nucleation in tropical tropopause layer cirrus, Geophys. Res. Lett., 43, 6629–6635, https://doi.org/10.1002/2016GL069426, 2016.

Jensen, E. J., Ueyama, R., Pfister, L., and Atlas, R. L.: The Impacts of Gravity Waves and Wind Shear on the Lifecycle of Cirrus Clouds in the Tropical Tropopause Layer, J. Geophys. Res., 130, https://doi.org/10.1029/2024jd042308, 2025.

Jensen, E. J., Corcos, M., and Kärcher, B.: Influence of Variations in Gravity Wave Properties on Cirrus Ice Number Concentrations Produced by Homogeneous Freezing in the Tropical Tropopause Layer, J. Geophys. Res., 131, https://doi.org/10.1029/2025jd044467, 2026.

Kim, J.-E., Alexander, M. J., Bui, T. P., Dean-Day, J. M., Lawson, R. P., Woods, S., Hlavka, D., Pfister, L., and Jensen, E. J.: Ubiquitous influence of waves on tropical high cirrus clouds, Geophys. Res. Lett., 43, 5895–5901, https://doi.org/10.1002/2016gl069293, 2016.

Koop, T., Luo, B., Tsias, A., and Peter, T.: Water activity as the determinant for homogeneous ice nucleation in aqueous solutions, Nature, 406, 611–614, https://doi.org/10.1038/35020537, 2000.

Kottayil, A., Podglajen, A., Legras, B., Atlas, R., K, P., Satheesan, K., and S, A.: High-Frequency Gravity Waves and Kelvin-Helmholtz Billows in the Tropical UTLS, as Seen From Radar Observations of Vertical Wind, Geophysical Research Letters, 51, e2024GL110 366, https://doi.org/https://doi.org/10.1029/2024GL110366, e2024GL110366 2024GL110366, 2024.

Kärcher, B.: Simulating gas-aerosol-cirrus interactions: Process-oriented microphysical model and applications, Atmos. Chem. Phys., pp. 1645–1664, https://doi.org/10.5194/acp-3-1645-2003, 2003.

Kärcher, B. and Corcos, M.: On processes affecting lifetimes of persistent contrails and contrail cirrus., J. Geophys. Res., in review, 2025.

Kärcher, B. and Podglajen, A.: A Stochastic Representation of Temperature Fluctuations Induced by Mesoscale Gravity Waves, J. Geophys. Res., 124, 11 506–11 529, https://doi.org/10.1029/2019jd030680, 2019.

Kärcher, B., Hoffmann, F., Sokol, A. B., Gasparini, B., Corcos, M., Jensen, E., Atlas, R., Podglajen, A., Morrison, H., Hertzog, A., Plougonven, R., Chandrakhar, K. K., and Grabowski, W. W.: Dissecting cirrus clouds: navigating effects of turbulence on homogeneous ice formation, npj Climate and Atmospheric Science, 8, https://doi.org/10.1038/s41612-025-01024-w, 2025.

LATMOS/IPSL: BeCOOL Lidar Level 1 and 2, V3, https://doi.org/10.14768/bad47567-f844-4084-abd9-917668e18d82, 2024.

Lesigne, T., Ravetta, F., Podglajen, A., Mariage, V., and Pelon, J.: Extensive coverage of ultrathin tropical tropopause layer cirrus clouds revealed by balloon-borne lidar observations, Atmos. Chem. Phys., 24, 5935–5952, https://doi.org/10.5194/acp-24-5935-2024, 2024.

Lesigne, T., Podglajen, A., and Ravetta, F.: Tropical Cirrus Lifetime Estimated From Superpressure Balloon-Borne Lidar Observations, Geophys. Res. Lett., 52, https://doi.org/10.1029/2025gl117353, 2025.

Liou, K. N., Ou, S. C., Takano, Y., Valero, F. P. J., and Ackerman, T. P.: Remote Sounding of the Tropical Cirrus Cloud Temperature and Optical Depth Using 6.5 and 10.5 $\mu$m Radiometers during STEP, J. Applied Meteo., 29, 716–726, https://doi.org/10.1175/1520-0450(1990)029<0716:rsottc>2.0.co;2, 1990.

https://doi.org/10.5194/egusphere-2026-3112
Preprint. Discussion started: 10 July 2026


Lolli, S., Campbell, J. R., Lewis, J. R., Gu, Y., and Welton, E. J.: Technical note: Fu–Liou–Gu and Corti–Peter model performance evaluation for radiative retrievals from cirrus clouds, Atmos. Chem. Phys., 17, 7025–7034, https://doi.org/10.5194/acp-17-7025-2017, 2017.

Luo, B. P., Peter, T., Wernli, H., Fueglistaler, S., Wirth, M., Kiemle, C., Flentje, H., Yushkov, V. A., Khattatov, V., Rudakov, V., Thomas, A., Borrmann, S., Toci, G., Mazzinghi, P., Beuermann, J., Schiller, C., Cairo, F., Di Don-Francesco, G., Adriani, A., Volk, C. M., Strom, J., Noone, K., Mitev, V., MacKenzie, R. A., Carslaw, K. S., Trautmann, T., Santacesaria, V., and Stefanutti, L.: Ultrathin Tropical Tropopause Clouds (UTTCs): II. Stabilization mechanisms, Atmos. Chem. Phys., 3, 1093–1100, https://doi.org/10.5194/acp-3-1093-2003, 2003.

McFarquhar, G. M., Heymsfield, A. J., Spinhirne, J., and Hart, B.: Thin and Subvisual Tropopause Tropical Cirrus: Observations and Radiative Impacts, J. Atmos. Sci., 57, 1841–1853, https://doi.org/10.1175/1520-0469(2000)057<1841:tasttc>2.0.co;2, 2000.

Pfister, L., Selkirk, H. B., Jensen, E. J., Schoeberl, M. R., Toon, O. B., Browell, E. V., Grant, W. B., Gary, B., Mahoney, M. J., Bui, T. V., and Hintsa, E.: Aircraft observations of thin cirrus clouds near the tropical tropopause, J. Geophys. Res., 106, 9765–9786, https://doi.org/10.1029/2000jd900648, 2001.

Podglajen, A., Hertzog, A., Plougonven, R., and Legras, B.: Lagrangian temperature and vertical velocity fluctuations due to gravity waves in the lower stratosphere, Geophys. Res. Lett., 43, 3543–3553, https://doi.org/10.1002/2016GL068148, 2016.

Podglajen, A., Plougonven, R., Hertzog, A., and Jensen, E.: Impact of gravity waves on the motion and distribution of atmospheric ice particles, Atmos. Chem. Phys., pp. 10 799–10 823, https://doi.org/10.5194/acp-18-10799-2018, 2018.

Randel, W. J., Wu, F., and Podglajen, A.: Equatorial Waves, Diurnal Tides and Small-Scale Thermal Variability in the Tropical Lower Stratosphere From COSMIC-2 Radio Occultation, J. Geophys. Res., 126, https://doi.org/10.1029/2020jd033969, 2021.

Schoeberl, M. R., Jensen, E., Podglajen, A., Coy, L., Lodha, C., Candido, S., and Carver, R.: Gravity wave spectra in the lower stratosphere diagnosed from project loon balloon trajectories, J. Geophys. Res., 122, 8517–8524, https://doi.org/10.1002/2017jd026471, 2017.

Spichtinger, P. and Krämer, M.: Tropical tropopause ice clouds: a dynamic approach to the mystery of low crystal numbers, Atmos. Chem. Phys., 13, 9801–9818, https://doi.org/10.5194/acp-13-9801-2013, 2013.

Sweeney, A. J. and Fu, Q.: Interannual Variability of Temperature, Water Vapor, and Clouds in the Tropical Tropopause Layer, Authorea, https://doi.org/10.22541/essoar.168167390.09887630/v1, 2023.

Thornberry, T. D., Rollins, A. W., Avery, M. A., Woods, S., Lawson, R. P., Bui, T. V., and Gao, R.-S.: Ice water content-extinction relationships and effective diameter for TTL cirrus derived from in situ measurements during ATTREX 2014, J. Geophys. Res., 122, 4494–4507, https://doi.org/10.1002/2016jd025948, 2017.

van de Hulst, H. C.: Light scattering by small particles, 1981.

Wright, C. J., Osprey, S. M., and Gille, J. C.: Global observations of gravity wave intermittency and its impact on the observed momentum flux morphology, J. Geophys. Res., 118, 10,980–10,993, https://doi.org/10.1002/jgrd.50869, 2013.